Pressure drop for adiabatic air-water flow through a time-varying constriction

A. Van Hirtum, A. Bouvet, and X. Pelorson

Citation: Physics of Fluids **30**, 101901 (2018); doi: 10.1063/1.5049765
View online: https://doi.org/10.1063/1.5049765
View Table of Contents: http://aip.scitation.org/toc/phf/30/10
Published by the American Institute of Physics

Pressure drop for adiabatic air-water flow through a time-varying constriction

A. Van Hirtum,[a] A. Bouvet, and X. Pelorson
LEGI, UMR CNRS 5519, Grenoble Alpes University, Grenoble, France

(Received 25 July 2018; accepted 8 October 2018; published online 25 October 2018)

The pressure drop for air-water flow within a vertical rigid channel containing a severe time-varying constriction is studied for different forcing frequencies $f_c \in \{1, 6, 10\}$ Hz after water (0 up to 5 ml) is injected upstream. The pressure drop at the minimum aperture is observed experimentally and can be modeled with a quasi-steady one-dimensional approach and viscous mixing during the closing and opening phase. It is found that the flow can be regarded as gas dominated during the closing phase. During the opening phase, mixing enhances as $f_c > 1$ Hz, which emphasizes the contribution of water and water droplets to the viscous mixture. Eventually, for $f_c = 10$ Hz and greater water volumes (≥3 ml), mixing is further increased so that the flow becomes homogeneous and turbulent during the opening phase. Assessed conditions are relevant to flow through the human glottis. *Published by AIP Publishing.* https://doi.org/10.1063/1.5049765

I. INTRODUCTION

Respiratory flow through the human upper airways and, in particular, through the glottis, i.e., airway constriction formed between both vocal folds within the larynx, is often studied considering single-phase airflow through a uniform rigid channel containing a time-varying constriction, as illustrated in Fig. 1. As such, the presence of liquid in the fluid is generally neglected.[10,13,35,37] However, this assumption of single-phase airflow is in contrast to the physiological reality and is reported to affect flow-induced phenomena such as the shown effect of surface (de-)hydration on human voiced speech sound production.[1,17,36]

When the presence of liquid is accounted for, adiabatic two-phase gas-liquid flow occurs. It is well established that the mixture viscosity of gas-liquid two-phase flow strongly influences the pressure drop and thus the forces exerted by the flow on the surrounding channel walls driving fluid-structure interactions and associated phenomena such as voiced speech sound production, brass instruments play, whistling, etc.

As liquid is added, the viscosity of the gas-liquid mixture increases and hence it is expected that the pressure gradient rises.[20] Nevertheless, studies of adiabatic gas-liquid flow mostly focus on steady flow through uniform channels[3,40] whereas a channel with time-varying constriction degree is more pertinent for glottal flow during speech production. Although it has been shown from a dimensional analysis[10,35,37] of single-phase airflow under glottal conditions (Reynolds number $Re \leq 5 \times 10^3$, Strouhal number $Sr \leq 0.1$, and Mach number $Ma \leq 0.12$) that incompressible, laminar, and quasi-steady flow can be considered, the presence of a time-varying constriction and hence pulsating jet might affect the mixture viscosity. Indeed, enhanced mixing is reported for intermittent liquid injection which is particularly the case during and after a deceleration phase as occurs for engine jets.[19,29] In the case of a sinusoidally time-varying constriction, flow deceleration occurs during the opening phase of the oscillatory cycle. Consequently, besides the effect of gas-liquid flow on the pressure drop, effects of the forcing frequency on mixing and hence on the mixture viscosity need to be studied as well. It is noted that near closure viscous flow effects are shown to provide a major contribution to the pressure gradient when single-phase airflow through a glottal-like constriction is considered.[10,13,35,37] Therefore, the aim of this work is twofold. First, it is sought to provide experimental evidence of the effect of two-phase flow and of the imposed oscillation frequency f_c on pressures P_c measured at the minimum constriction for different upstream punctually injected water volumes V_L (Fig. 1) ranging from dry to excessive. Second, it is sought to accurately model observed pressures P_c applying a quasi-steady one-dimensional flow model approach for assessed (f_c, V_L) cases while accounting for viscous mixing. Since different surface hydration conditions occur for glottal flow (due to smoking, drinking, gurgling, etc.), both gas and liquid ruled viscous mixing are considered. In the following, the model (Sec. II) and experimental (Sec. III) approaches are outlined. Next, experimental and model results are presented in Sec. IV, and the conclusion is formulated in Sec. V.

II. MODEL APPROACH

A. Pressure drop with single-phase viscous contribution

Single-phase flow of a fluid with density ρ and dynamic viscosity μ through a constricted channel is modeled following the quasi-one-dimensional approach outlined in Refs. 10, 34, and 39. The model assumes quasi-steady laminar incompressible pressure driven flow while accounting for boundary layer development due to viscosity within the constricted channel portion. An empirical *ad hoc* geometrical criterion is used to indicate the streamwise position of flow separation and jet

[a]Electronic mail: annemie.vanhirtum@univ-grenoble-alpes.fr

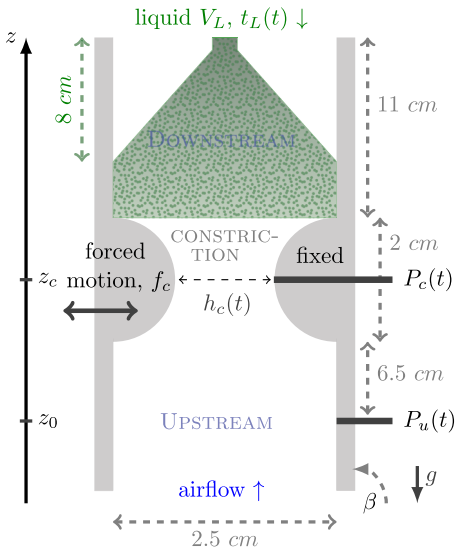

FIG. 1. Schematic overview of the vertical ($\beta = 90°$) rigid channel with time-varying rectangular constriction (radius 1 cm, width $l_c = 3.0$ cm), pressure taps, and fluid supplies: orientation angle β, gravitational acceleration g, imposed mobile vocal fold frequency f_c, time-varying minimum spacing $h_c(t)$, liquid supply time tag $t_L(t)$, liquid volume V_L, upstream pressure $P_u(t)$, and minimum constriction pressure $P_c(t)$. Flow is supplied along the positive z-direction, and liquid is injected along the negative z-direction.

formation z_s along the diverging side of the constriction ($z \geq z_c$) as the area corresponding to $A_s = c_s \cdot A_c$ with separation constant $c_s \geq 1$ and minimum channel area A_c. Concretely, the constant is set to $c_s = 1.13$ given the constriction geometry which is within the range commonly reported in the literature[8–10,35] for glottal-like geometries ($1.05 \leq c_s \leq 1.4$).

To overcome the constraint of a horizontal flow channel, the model is altered to account for gravitational flow acceleration g for any given channel orientation angle β, with $\beta = 0°$ and $\beta = 90°$ for a horizontal and vertical channel, respectively (Fig. 1). The pressure distribution within the channel with time-varying area $A(z, t)$ as a function of streamwise position z and time t up to flow separation ($z_0 \leq z \leq z_s$) becomes

$$P(z,t) = P_u(t) + \frac{1}{2}\rho\Phi^2(t)\left(\frac{1}{A^2(z_0)} - \frac{1}{A^2(z,t)}\right) + \mu\Phi\int_{z_0}^{z}\frac{dz}{\alpha(z,t)} + \rho g\sin(\beta)(z_0 - z). \quad (1)$$

The function $\alpha(z, t)$ in the term describing the viscous contribution to the pressure drop (third right-hand term) depends on the channel's cross section shape within the constriction.[34,39] For a rectangular cross section shape with constant width w and varying height $h(z, t)$, a two-dimensional Poiseuille flow assumption can be applied when $w \gg h_c$ in the constricted portion,

$$\alpha(z,t) = -\frac{w \cdot h^3(z,t)}{12}.$$

At flow separation ($z = z_s$ and $A = A_s$), $P(z_s, t) = P_d$, with downstream pressure $P_d = 0$ so that volume flow velocity Φ can be estimated from (1),

$$\Phi(t) = \left[\mu\int_{z_0}^{z_s}\frac{dz}{\alpha(z,t)} + \left\{\left(\mu\int_{z_0}^{z_s}\frac{dz}{\alpha(z,t)}\right)^2 + 2\rho\Big((P_u(t) - P_d) + \rho g\sin(\beta)(z_0 - z_s(t))\Big) \times \left(\frac{1}{A^2(z_s,t)} - \frac{1}{A^2(z_0)}\right)\right\}^{1/2}\right]\left[\rho\left(\frac{1}{A^2(z_s,t)} - \frac{1}{A^2(z_0)}\right)\right]^{-1}. \quad (2)$$

Once $\Phi(t)$ is known, $P(z, t)$ along the constricted channel portion is estimated using (1). The term describing the viscous pressure drop contribution in (1) and (2) needs to be reconsidered when a two-phase air-water mixture occurs. This is assessed in Sec. II B.

B. Two-phase viscous pressure drop contribution of air-water mixture

1. Homogeneous mixture

When no slip is assumed between the two phases of the air-water mixture, there is no velocity difference between the gas (air) and liquid (water) phase so that the fluid is considered homogeneous.[20] The flow is then regarded as a single-phase flow of a fluid having average properties determined by the gas-liquid mixing quality. Consequently, the one-dimensional model presented in Sec. II A can be applied and the two-phase pressure drop is again expressed as the sum of inertial (accelerational or decelerational), frictional, and gravitational components (1) when averaged mixture properties, density $\rho = \rho_h$ and dynamic viscosity $\mu = \mu_h$, can be determined in terms of the gas (subscript G) and liquid (subscript L) properties.

The homogeneous density is estimated as

$$\rho_h = \left(\frac{x}{\rho_G} + \frac{1-x}{\rho_L}\right)^{-1} \quad (3)$$

in terms of the mass quality x ($0 \leq x \leq 1$) so that homogeneous void (or gas) fraction $v_f = \frac{\Phi_G}{\Phi_G + \Phi_L}$ becomes

$$v_f = \frac{1}{1 + \left(\frac{1-x}{x}\right)\left(\frac{\rho_G}{\rho_L}\right)}, \quad (4)$$

with $0 \leq v_f \leq 1$. Consequently, $v_f = 0$ and $x = 0$ when $\Phi_G = 0$ (pure liquid flow) and $v_f = 1$ and $x = 1$ when $\Phi_L = 0$ (pure gas flow). From Fig. 2, it is seen that air-water flow at

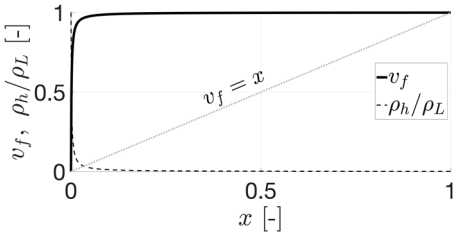

FIG. 2. Void fraction v_f (thick full line) and normalised homogeneous density ρ_h/ρ_L (thin dashed line) as a function of mass quality x for air-water mixture. As a reference, $v_f = x$ (diagonal line) for $\rho_L = \rho_G = \rho_h$ is indicated.

room temperature (density ratio $\rho_L/\rho_G \approx 832$) is gas dominated $v_f \geq 0.99$ ($\Phi_L \leq 0.01\Phi_G$ and $\rho_h \approx \rho_G$) for $x \geq 0.1$ compared to $x \geq 0.99$ for an equal density mixture ($\rho_L/\rho_G \approx 1$). It is observed that for $x < 0.01$, void fraction v_f decreases rapidly as ρ_h/ρ_L increases at the same rate so that the contribution of the liquid to the mixture properties gains importance and will finally dominate $v_f \leq 0.5$ ($\Phi_L \geq 0.5\Phi_G$ and $\rho_h \geq 0.5\rho_L$) as x and hence v_f further reduces towards 0.

Many averaging methods have been described in the literature to determine homogeneous mixture viscosity μ_h. The most straightforward approximations[12,18,31] assume that the flow is liquid dominated. In order to account for liquid as well as gas phase dominated flow, it is proposed to reformulate these models more generally so that μ_h is estimated based on the viscosity of a single phase, either gas ($i = G$) or liquid ($i = L$), as

$$\mu_h = \mu_i \cdot \alpha_{\mu,i}, \tag{5}$$

with scaling factor $\alpha_{\mu,i}$. To account for the dominant phase i as well as a non-unity density ratio between the phases, scaling factor $\alpha_{\mu,i} = \frac{\rho_h}{\rho_i}$ is introduced following Garcia *et al.*[18] Following Davidson *et al.*,[12] scaling factor $\alpha_{\mu,i} = \left[1 - x^{(r)}(1-x)^{(1-r)}\left(\frac{\rho_i}{\rho_j} - 1\right)\right]$ ($\forall r \in \{0, 1\}$) is proposed with j indicating the non-dominant phase, i.e., $j = L$ for $i = G$ and $j = G$ for $i = L$ and exponent $r = 0$ for gas dominated flow and $r = 1$ for liquid dominated flow. This way, μ_i is scaled explicitly by mass quality x and single phase density ratio ρ_i/ρ_j. For liquid dominated flow ($r = 1$), the original expression given in Ref. 12 is retrieved. As expected, $\alpha_{\mu,i} = 1$ holds for pure liquid ($x = 0$) or pure gas ($x = 1$) flow. So that following Owen[31] for single phase dominated flows, a constant unity scaling factor ($\alpha_{\mu,i} = 1$) is assumed. Used scaling factors $\alpha_{\mu,i}$ in (5), i.e., $f(\rho_h/\rho_i)$ (thin dashed line), $f(\rho_i/\rho_j, x)$ (thick full line), and unity constant ($cte = 1$, horizontal dashed line), as a function of x are illustrated in Fig. 3 for air-water flow. It is verified that scaling factor $\alpha_{\mu,i=L}$ decreases from 1 ($\alpha_{\mu,i=L} \leq 1$) for liquid ruled flows so that mixture viscosity μ_h reduces compared to μ_L as gas is added. On the other hand, scaling factor $\alpha_{\mu,i=G}$ increases from 1 ($\alpha_{\mu,G} \geq 1$) as liquid is added for gas ruled flow so that mixture viscosity μ_h augments from μ_G. Decreasing (for liquid ruled) and increasing (for gas ruled) scaling factor $\alpha_{\mu,i}$, and hence increasing and decreasing mixture viscosity following (5), with increased air-water mixing aims to reduce the viscosity difference ($\mu_L \gg \mu_G$) between pure water ($\mu_L \approx 1.0 \times 10^{-3}$ Pa s) and pure air ($\mu_G \approx 1.8 \times 10^{-5}$ Pa s) flow. Nevertheless, estimating mixture viscosity μ_h by scaling, the viscosity of the gas or liquid phase (5) loses its motivation as mixing increases since the underlying assumption of single-phase dominated flow ebbs away.

To obtain μ_h estimations which are also valid in the transition zone between liquid and gas single-phase ruled flows, μ_h models using the viscosity of both phases, i.e., μ_L and μ_G, are proposed in the literature.[2,4,7,14,15,25,27] A common approach is to express mixing viscosity μ_h (exponent $s = 1$) or its reciprocal ($s = -1$) as a sum of single-phase viscosities or their inverses weighted by scaling factors γ_L (for μ_L) and γ_G (for μ_G) as

$$\mu_h^{(s)} = \mu_L^{(s)} \cdot \gamma_L + \mu_G^{(s)} \cdot \gamma_G + \gamma_0, \quad \forall s \in \{-1, 1\}, \tag{6}$$

with offset $\gamma_0 = 0$ when not explicitly stated. The earliest—and most common[11]—models defined scaling factors as mass averages the same way as for ρ_h in (3), i.e., $\gamma_G = x$ and $\gamma_L = 1 - x$ according to McAdams *et al.*[27] (for $s = -1$) and Cicchitti *et al.*[7] (for $s = 1$). This scaling is further refined to account besides the mass quality also for densities of the phases which involves void fraction v_f following Beattie and Whalley[4] (for $s = 1$) since $\gamma_G = v_f$ and $\gamma_L = (1 - v_f)(1 + 2.5v_f)$ and kinematic viscosities of the flow phases following Dukler *et al.*[14] (for $s = 1$) since $\gamma_G = \rho_h x/\rho_G$ and $\gamma_L = \rho_h(1 - x)/\rho_L$ to which Fourar and Bories[15] (for $s = 1$) added $\gamma_0 = 2\sqrt{x(1-x)\mu_G\mu_L/\rho_G\rho_L}$, which is maximum for $x = 0.5$ and reduces symmetrical towards 0 at limiting values $x \in \{0, 1\}$ so that μ_h is increased for intermediate x compared to values obtained for $\gamma_0 = 0$. Furthermore, Lin *et al.*[25] (for $s = -1$) optimized (for data in $0 < x < 0.25$) scaling factors provided by McAdam *et al.*[27] by adding an exponent greater than unity to the mass averaging so that resulting μ_h increases as $\gamma_G = x^{1.4}$ and $\gamma_L = (1 - x^{1.4})$. It is noted that (6) satisfies limiting conditions $\mu_h = \mu_L$ and $\mu_h = \mu_G$ for pure liquid ($x = 0$) and pure gas flow ($x = 1$), which is not the case for (5). Homogeneous air-water mixture viscosity μ_h from (6) normalized by μ_L obtained for different scaling factors γ_L and γ_G (and $\gamma_0 = 0$) is plotted in Fig. 4 as a function of x. It is seen that μ_h estimated using (6) decreases continuously as gas concentration (and hence x) is raised. Nevertheless important differences in the mixing viscosity are observed depending on the scaling factors and offset extending (Beattie, Dukler) or shortening (Cicchitti, Lin) the range of gas dominated flow compared to values obtained by applying (5) with scaling

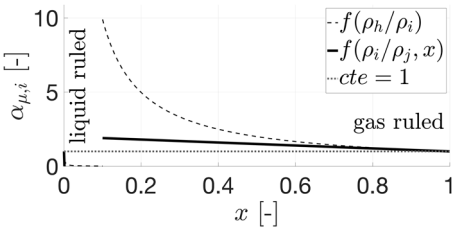

FIG. 3. Scaling factors $\alpha_{\mu,i}$ in (5) for gas ($i = G$) and liquid ($i = L$) ruled flows as a function of x for air-water mixture: $\alpha_{\mu,i} = f(\rho_h/\rho_i)$ (thin dashed line), $\alpha_{\mu,i} = f(\rho_i/\rho_j, x)$ (thick full line), and unity $\alpha_{\mu,i} = 1$ (horizontal dotted line).

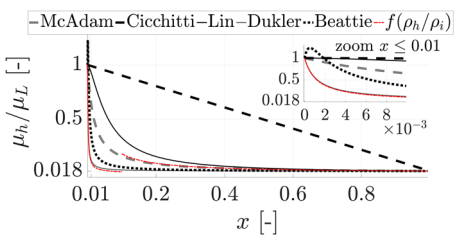

FIG. 4. Normalised homogeneous mixing viscosity $\mu_h(x)/\mu_L$ from (6) for air-water mixture with (γ_L, γ_G) following McAdam (gray thick dashed), Cicchitti (black diagonal thick dashed), Lin (black thick full), Dukler (gray thin full), and Beattie (black thick dotted). In addition, $\mu_h(x)/\mu_L$ from (5) with Garcia [$f(\rho_h/\rho_i)$, discontinuous thin dashed-dotted] is shown. Note that $\mu_G/\mu_L \approx 0.018$. A zoom for $x \leq 0.01$ is included.

factor $f(\rho_h/\rho_i)$ which is in close approximation with McAdam's curve for gas dominated flow and with Dukler's curves for liquid dominated flow. It was noted that Dukler's ($\gamma_0 = 0$) and Fourar's ($\gamma_0 > 0$) curves overlap so that Fourar's curve is not considered and $\gamma_0 = 0$ holds.

Mixing viscosity μ_h from (6) or (5) neglects turbulence. Nevertheless, in the case of gas-liquid flows, the homogeneous flow assumption is most suitable to describe flow with bubbles or droplets which induces turbulence. Therefore, it is sought to model μ_h while accounting for turbulence in addition to the fluid characteristics of the phases and their concentration. Turbulent mixing viscosity μ_h^τ for liquid dominated homogeneous flow[22] is extended to single-phase ruled homogeneous flow in general as

$$\mu_h^\tau = \mu_h + \mu_\tau = \gamma_\tau \cdot \alpha_{\mu,i} \cdot \mu_i, \text{ with } 1 < \gamma_\tau, \tag{7}$$

with turbulent viscosity μ_τ, subscript $i \in \{G, L\}$ indicating as before the dominating phase, scaling factor $\alpha_{\mu,i}$ as defined in (5), and introducing turbulent scaling factor $\gamma_\tau > 1$. For homogeneous flow, it is shown[22,32] that γ_τ depends on the bubble/droplet size so that $1.1 \leq \gamma_\tau \leq 2$. Aung and Yuwono[2] proposed to apply the same approach of single-phase ruled flow to flows with intermediate gas and liquid concentrations so that following their approach, (6) becomes

$$\left(\mu_h^\tau\right)^{(s)} = \gamma_\tau^{(s)}\left(\mu_L^{(s)} \cdot \gamma_L + \mu_G^{(s)} \cdot \gamma_G + \gamma_0\right), \quad \forall s \in \{-1, 1\}, \tag{8}$$

which can be applied for all void fractions v_f. A common value[2] yields $\gamma_\tau = 1.7$ so that turbulent mixing viscosity μ_h^τ is increased with 70% compared to mixing viscosity μ_h for the same scaling factors $\{\gamma_L, \gamma_G, \gamma_0\}$. Concretely, Aung[2] proposed to use maximized viscosity μ_h^τ regardless of x by applying (7) with $\alpha_{\mu,L} = 1$ for liquid ruled flow[31] ($0 \leq x < x_{thres}$) and (8) with $\{\gamma_L, \gamma_G, \gamma_0\}$ following Cicchitti[7] elsewhere ($x_{thres} \leq x \leq 1$),

$$\begin{aligned} \mu_h^\tau &= 1.7 \cdot \mu_L, \quad 0 \leq x < x_{thres}, \\ \mu_h^\tau &= 1.7(x \cdot \mu_G + (1-x)\mu_L), \quad x_{thres} \leq x \leq 1, \end{aligned} \tag{9}$$

with concentration threshold $0 < x_{thres} < 1$. Turbulent mixing viscosity μ_h^τ for air-water flow obtained from (9) with $x_{thres} = 0.1$ is illustrated in Fig. 5. For intermediate x-values ($x \approx 0.5$), μ_h^τ yields by definition from 1.7 up to 25 times μ_h from (6) with $\{\gamma_L, \gamma_G, \gamma_0\}$ taken following Cicchitti[7] and McAdams,[27] respectively, so that the contribution of turbulence is most notable for intermediate x-values.

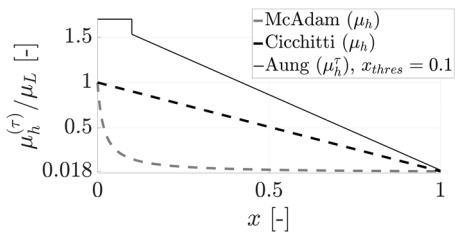

FIG. 5. Normalised homogeneous mixing viscosity $\mu_h(x)/\mu_L$ from (6) [McAdam (gray thick dashed) and Cicchitti (black diagonal thick dashed)] and turbulent mixing viscosity μ_h^τ/μ_L from (9) [Aung (black thin full)] for air-water mixture.

2. Separated flow model for air-water mixture

When the assumption of no slip between the phases is dropped, velocities of both phases might be different so that the homogeneous flow model is no longer valid and (4) becomes

$$v_f = \frac{1}{1 + S\left(\frac{1-x}{x}\right)\left(\frac{\rho_G}{\rho_L}\right)}, \tag{10}$$

with S indicating the slip between both phases. In order to apply the one-dimensional model approach in Sec. II A, the viscous contribution to the pressure drop is modeled considering both phases as separated streams independently of the flow regime.[20] The slip is then accounted for using empirical liquid hold up correlations and empirical relations describing the frictional interaction between the phases. Slip can be accounted for following two-phase friction multipliers ϕ_L^2 and ϕ_G^2 proposed in a landmark paper by Lockhart and Martinelli[26] which relates frictional two-phase pressure drop $\Delta P_{f,M}$ and frictional pressure drops $\Delta P_{f,i\in\{L,G\}}$, which would exist if the gas ($i = G$) or liquid ($i = L$) phase is assumed to flow alone,

$$\Delta P_{f,M} = \phi_L^2 \cdot \Delta P_{f,L}, \tag{11}$$

$$\Delta P_{f,M} = \phi_G^2 \cdot \Delta P_{f,G}. \tag{12}$$

Multipliers $\phi_L^2, \phi_G^2 \geq 1$ can be determined following fitted correlations in the work of Chisholm,[5]

$$\phi_L^2 = 1 + \frac{C_{LG}}{X} + \frac{1}{X^2}, \tag{13}$$

$$\phi_G^2 = 1 + C_{LG}X + X^2, \tag{14}$$

with Martinelli's parameter X defined as a decreasing function of x,

$$X = \left(\frac{1-x}{x}\right)^{0.9}\left(\frac{\rho_G}{\rho_L}\right)^{0.5}\left(\frac{\mu_L}{\mu_G}\right)^{0.1}, \tag{15}$$

and Chisholm's constant C_{LG} depending on the liquid-gas flow regime: $C_{LG} = 5$ for laminar-laminar (LL) flow, $C_{LG} = 10$ for turbulent-laminar (TL) flow, $C_{LG} = 12$ for laminar-turbulent (LT) flow, and $C_{LG} = 20$ for turbulent-turbulent (TT) flow. Multipliers as a function of X for different Chisholm's constants are shown in Fig. 6. It is seen that gas flow occurs for $X \ll 1$ ($\phi_L^2 \to \frac{1}{X^2}$, $\phi_G^2 \to 1$), liquid flow occurs for $X \gg 100$ ($\phi_L^2 \to 1$, $\phi_G^2 \to X^2$), and two-phase flow occurs for intermediate X-values ($\phi_L^2 \approx f(X)$, $\phi_G^2 \approx f(X)$). Different C_{LG} values are reported on as shown correlations provide a one-parameter data-fitting problem for C_{LG} in an attempt to reflect the effect of the flow regime and channel geometry (e.g., cross section shape, hydraulic diameter, orientation angle) with more accuracy.[6,16,23,24,30,33,40–42] The meaning of constant C_{LG} is seen writing

$$\Delta P_{f,M} = \Delta P_{f,L} + C_{LG}\left(\Delta P_{f,L} \cdot \Delta P_{f,G}\right)^{1/2} + \Delta P_{f,G}, \tag{16}$$

indicating that the interfacial contribution to the total frictional two phase pressure drop is

$$\Delta P_{\mathcal{I},M} = C_{LG}\left(\Delta P_{f,L} \cdot \Delta P_{f,G}\right)^{1/2} \tag{17}$$

so that C_{LG} weights the mean of the contribution of pure gas and liquid to $\Delta P_{\mathcal{I},M}$. Furthermore, C_{LG} can be derived

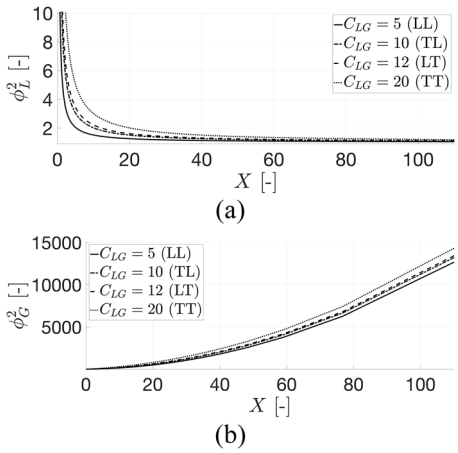

FIG. 6. Multipliers ϕ_L^2 (a) and ϕ_G^2 (b) as a function of Martinelli's parameter X for air-water flow ($\rho_L/\rho_G = 832$) and for different Chisholm's constants: $C_{LG} = 5$ for laminar-laminar (LL) flow (full line), $C_{LG} = 10$ for turbulent-laminar (TL) flow (dashed-dotted line), $C_{LG} = 12$ for laminar-turbulent (LT) flow (dashed line), and $C_{LG} = 20$ for turbulent-turbulent (TT) flow (dotted line).

analytically[38] under certain flow assumptions. For homogeneous air-water flow, $C_{LG} \approx 28.6$ which agrees well with Chisholm's value for turbulent-turbulent flow ($C_{LG} = 20$). For $C_{LG} = 0$, $\Delta P_{\mathcal{I},M}$ is the sum of the pressure drops of the single-phase flows corresponding to laminar plug flow. A continuous expression of C_{LG} for air-water flow in vertical channels is proposed by Mishima and Hibiki,[28]

$$C_{LG} = 21\Big(1 - \exp(-0.319D)\Big), \tag{18}$$

and later refined for adiabatic gas-liquid flow by Zhang *et al.*[41] as

$$C_{LG} = 21\Big(1 - \exp(-0.674/Lp)\Big), \tag{19}$$

as a function of Laplace number Lp,

$$Lp = \frac{\sqrt{\sigma/g(\rho_L - \rho_G)}}{D}, \tag{20}$$

with surface tension σ and hydraulic diameter D. For air-water flow at temperature $T \approx 22\,^{\circ}$C and assuming $D \leq 3$ mm, $\sigma \approx 72$ mN/m (at temperature $T = 22 \pm 2\,^{\circ}$C), it follows from (20) that $Lp > 0.9$ so that (19) $C_{LG} \leq 11$ holds, as plotted in Fig. 7. Therefore from (19), it follows that C_{LG} increases with D and is in fair agreement with Chisholm's value for laminar-laminar flow ($C_{LG} = 5$) for $D \approx 1.1$ mm and for turbulent-laminar flow ($C_{LG} = 10$) for $D \approx 2.6$ mm. Note

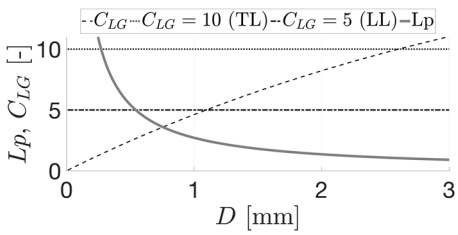

FIG. 7. C_{LG} (thin dashed line) constant (19) and Laplace number (thick full line) (20) for air-water flow ($\rho_L/\rho_G = 832$) as a function of hydraulic diameter D. As a reference constant, Chisholm's values for laminar-laminar (LL) flow ($C_{LG} = 5$) and for turbulent-laminar (TL) flow ($C_{LG} = 10$) are shown.

that $D < 3$ mm corresponds to micro-scale channels based on the classification of Kandlikar[21] using 3 mm as the threshold.

III. EXPERIMENTAL APPROACH

Experiments are performed by imposing a known time-varying constriction within a vertical rigid uniform circular channel (internal radius 12.5 mm), as schematically illustrated in Fig. 1. The constriction is obtained by inserting two rigid parallel half cylinders as depicted in Fig. 8 (radius 10 mm, constant width $l_c = 30$ mm), one of which is fixed and one of which is mobile by applying a forced motion.[10,13,37] Sinusoidal movement of the rectangular gap between both half cylinders is imposed with forcing frequency $f_c \in \{1, 6, 10\}$ Hz. Time-varying minimum constriction spacing $h_c(t)$ ($0 \leq h_c \leq 0.91$ mm) is measured by means of an optical sensor (OPB700, accuracy ±0.01 mm) so that the time-varying minimum area along the channel is obtained as $A_c(t) = h_c(t) \cdot l_c$. Consequently, during experiments, hydraulic diameter yields $D \leq 2$ mm and area constriction ratio $\mathcal{R}$ is sinusoidally varied between 100% and 95%.

Continuous steady airflow (density $\rho_G = 1.2$ kg m^{-3} and dynamic viscosity $\mu_G = 1.8 \times 10^{-5}$ Pa s, temperature $T = 22 \pm 2\,^{\circ}$C) is provided along the positive z-direction (Fig. 1) by a valve controlled air supply. Pressure transducers (Kulite XCS-093) are positioned in pressure taps upstream and at the minimum spacing so that upstream pressure P_u and minimum constriction pressure P_c are measured. Air supply is set so that in the absence of liquid, mean upstream pressure $\overline{P}_{up}$ yields 1136 ± 30 Pa regardless of f_c.

From a dimensional analysis, it follows that airflow through the time-varying constriction results in non-dimensional numbers characterizing airflow through the glottis of a male adult:[8,10,13,35,37] $Re \sim O(10^3)$, $Sr \sim O(10^{-2})$, $Ma \sim O(10^{-1})$. Non-dimensional numbers are either of the same order of magnitude or smaller when water is considered. In addition, the aspect ratio h_c/l_c of the time-varying constriction yields $h_c/l_c \ll 1$, as is observed for human subjects, which motivates the quasi-one-dimensional flow model approach. Consequently, flow assumptions underlying the model approach outlined in Sec. II A remain valid when considering airflow through the time-varying constriction shown in Fig. 1.

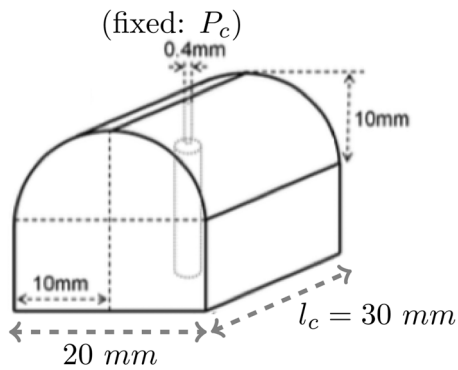

FIG. 8. Shape of the inserted fixed (with pressure tap P_c) and mobile (without pressure tap P_c) rigid half cylinders of the time-varying constriction shown in Fig. 1. The figure is based on Ref. 8.

TABLE I. Injected liquid volume V_L and duration Δt_L. Estimated flow rate Φ_L during injection.

V_L (ml)	1.0 ± 0.1	2.0 ± 0.1	3.0 ± 0.1	4.0 ± 0.1	5.0 ± 0.1
Δt_L (s)	0.86 ± 0.17	1.02 ± 0.10	1.47 ± 0.22	1.66 ± 0.27	2.61 ± 0.41
Φ_L (ml/s)	1.11 ± 0.11	1.98 ± 0.19	2.26 ± 0.22	2.15 ± 0.21	1.95 ± 0.19

Distilled water (density $\rho_L = 998$ kg m^{-3} and dynamic viscosity $\mu_L = 1.0 \times 10^{-3}$ Pa s, temperature $T = 22 \pm 2\,^{\circ}$C) is injected manually at the downstream end of the channel by emptying a graduated (accuracy 0.1) syringe equipped with a spray nozzle (diffusion angle 20° ± 1°, diameter 1 mm) containing a known volume $V_L \in \{1, 2, 3, 4, 5\}$ ml. Liquid is supplied homogeneously along the constricted area (Fig. 1). Furthermore, liquid injection is time-tagged t_L by manually operating an electrical switch. The mean duration of liquid injection Δt_L increases quadratically (the coefficient of determination $R^2 = 0.97$) with V_L and its overall value is less than 3 s regardless of V_L (Table I). Liquid supply volume flow rate Φ_L (Table I) is then approximated as the ratio $V_L/\Delta t_L$. The overall order of magnitude yields $\Phi_L \approx 1.8 \pm 0.6$ ml/s. All signals are sampled using a sampling frequency of 10 kHz. No water leakage was observed along the upstream or downstream channel end.

As an example, Fig. 9 illustrates measured data for $f_c = 1$ Hz and $V_L = 4$ ml as a function of time t near the instant of liquid injection. Imposed sinusoidally varying $h_c(t)$ is indicated at the bottom, and measured pressures $P_u(t)$ and $P_c(t)$ are plotted at the top. Time-tag t_L corresponds to an impulse whose width Δt_L indicates the duration of liquid injection so that pure air flow occurs before the impulse and air-water mixture is observed following the impulse onset. During each period of the shown signals, upstream pressure P_u varies sinusoidally so that its maximum is reached when h_c is small and minimum P_u corresponds to large aperture h_c. Next, it is seen that P_c reaches its maximum near closure ($h_c = 0$ mm), whereas P_c is negative during most of the open phase ($h_c > 0$ mm). Although these general tendencies are observed for each period of the plotted signals, i.e., before, during, or after liquid injection, close observation of Fig. 9 shows some important changes to P_c and to a less extent to P_u following liquid injection. One striking feature characterizing P_c (and which is found to a less extent on P_u) is the irregular appearance of P_c-spikes. This suggests that turbulence is induced due to the presence of droplets, which are visually observed upstream from the constricted channel portion following liquid injection for all assessed V_L. Differences observed comparing airflow and air-water mixture flow data are further detailed in Sec. IV A. To avoid transitional phenomena immediately following liquid injection ($t_L > 0$), in the remainder of this work, data are extracted 6 s after liquid injection is terminated.

IV. RESULTS AND DISCUSSION

A. Experimental observations

Examples of measured data are presented in order to provide a qualitative description of the effect of liquid injection for all assessed (f_c, V_L).

The impact of V_L on measured minimum constriction pressure P_c is illustrated in Fig. 10 for h_c imposed with forcing frequency $f_c = 10$ Hz. P_u varies less than 4% for all assessed V_L so that a single P_u-curve is plotted. During each period, gap h_c evolves through the following consecutive phases: open, closing, closed, opening, and again open. In general, the effect of V_L on P_c increases with increasing V_L. Besides irregular P_c-spikes due to the splashing of droplets throughout the closing phase, differences are observed for small apertures occurring near and during closure corresponding to $h_c \leq 0.5$ mm or constriction ratio $\mathcal{R} \geq 98\%$. During the closing phase, this is most notable when h_c goes to zero, i.e., just prior to complete closure, when P_c decreases more with increasing V_L (e.g., 38% more for $V_L \geq 3$ ml) whereas at the beginning of the opening phase, the accumulation of liquid during the closed phase results in an increase of P_c followed by a delayed steep decrease which therefore occurs for larger h_c. The extent to which described phenomena are observed varies from period to period, but in general increases with increased V_L. Note that droplet splashing near the gap (and hence spiking) is limited at the start of the opening phase since accumulated liquid downstream from the gap is likely to be evacuated by pulsating jet formation and associated starting vortex and shear-layer role-up at the onset of the opening phase.

The effect of forcing frequency f_c on pressure measurements is illustrated for $f_c \in \{1, 6, 10\}$ Hz in Fig. 11 for $V_L = 0$ ml and $V_L = 5$ ml. Without liquid injection [$V_L = 0$ ml in Fig. 11(a)], the effect of f_c variation on measured pressures P_u and P_c is most notable when h_c reaches towards zero, i.e., at the end of the closing phase as $h_c \leq 0.15$ mm ($\mathcal{R} \geq 99\%$), during complete closure ($h_c = 0$ mm) and at the start of the opening phase while $h_c \leq 0.43$ mm ($\mathcal{R} \geq 98\%$). When $f_c = 1$ Hz, P_u reflects the inverse tendencies imposed on h_c. This way, at first, P_u reaches a minimum associated with maximum aperture and next P_u increases monotonously while h_c decreases during the closing phase until maximum P_u is

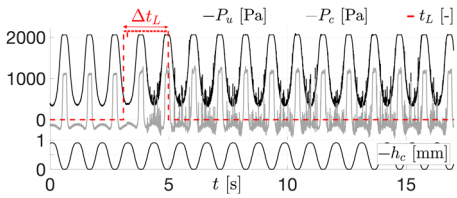

FIG. 9. Measured data for $f_c = 1$ Hz and $V_L = 4$ ml: (top) $P_u(t)$ (black full line), $P_c(t)$ (gray full line), and $t_L(t)$ (dashed line) with the duration of liquid injection Δt_L and (bottom) $h_c(t)$ (full line).

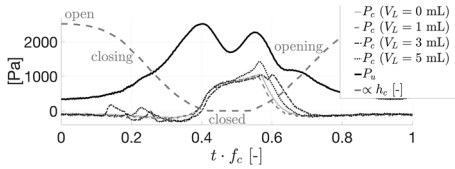

FIG. 10. Illustration of minimum constriction pressure P_c during a single period $t \cdot f_c$ ($f_c = 10$ Hz) for $V_L \in \{0, 1, 3, 5\}$ ml for given P_u and h_c (scaled with respect to P_u).

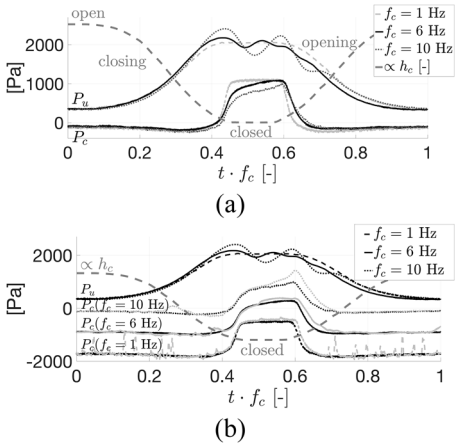

FIG. 11. Illustration of upstream pressure P_u and minimum constriction pressure P_c during a single period $t \cdot f_c$ for $f_c \in \{1, 6, 10\}$ Hz and prescribed h_c (scaled with respect to P_u): (a) $V_L = 0$ ml and (b) $V_L = 0$ ml (black curves) and $V_L = 5$ ml (gray curves). For clarity, P_c is shifted down for $f_c \in \{1, 6\}$ Hz.

maintained during the closed phase and afterwards P_u decreases monotonously to its minimum value as h_c increases during the opening phase. When f_c is increased ($f_c \in \{6, 10\}$ Hz), it is seen that P_u is no longer a monotonous function during the distinct phases since P_u fluctuates around the maximum value observed for $f_c = 1$ Hz following an increase (overshoot) just before complete closure, which causes P_u to fluctuate during the closed phase and start of the opening phase. The magnitude of the overshoot, resulting fluctuation, and affected h_c-range within each period increases with f_c, e.g., overshoot yields 6% for $f_c = 6$ Hz and 18% for $f_c = 10$ Hz. As a consequence for $f_c = 1$ Hz, $P_u = f(h_c)$ so that P_u and associated P_c during closing and opening phases are mirror-images of one another. For increased forcing frequency $f_c \in \{6, 10\}$, it is evident that this mirror-symmetry between the closing and opening phase does no longer exist for P_u and hence for P_c. The rate of P_c increase at the end of the closing phase is seen to decrease as P_u-overshoot increases with f_c.

During the subsequent closed phase and the start of the opening phase, the rate of P_c variation is dictated by the fluctuation of P_u. During the closed phase, this implies that P_c increases to a maximum at a rate which is either slowed down or accelerated as the amplitude of the P_u-fluctuation decreases or increases, respectively. The same way, during the start of the opening phase, the decrease of P_c is decelerated since P_u reduces more slowly. In addition, the minimum P_c value of the opening phase is greater than the minimum observed during the closing phase, i.e., the increase of 14% for $f_c = 6$ Hz and 25% for $f_c = 10\%$. Consequently, the main impact of increasing f_c for $V_L = 0$ ml lies in the breakdown of mirror-symmetry between the closing and opening phase for P_u and hence P_c.

To assess the effect of f_c on air-water mixture, flow ($V_L > 0$ ml) curves measured for $V_L \in \{0, 5\}$ ml and $f_c \in \{1, 6, 10\}$ Hz are plotted together in Fig. 11(b). As before, P_u is unaffected as V_L is varied so that a single curve is plotted for each f_c. To enhance clarity, P_c curves for $f_c = 6$ Hz and $f_c = 1$ Hz are shifted by extracting a constant offset of 800 Pa and 1600 Pa, respectively. It is seen that for $V_L > 0$ ml, irregular spikes in P_c are superposed on a smooth curve which varies from the one observed for $V_L = 0$ ml to an extent determined by f_c. Hence the effect of $V_L > 0$ ml on the curves observed for $V_L = 0$ ml is two-fold: on the one hand, irregular spikes occur due to the presence of droplet splashing near the constriction and on the other hand, the change of mixing flow properties during the period affects the smooth curve observed for $V_L = 0$ ml. It is noted that more spikes are seen as f_c reduces since the physical time corresponding to one period is greater (varies between 1 s and 0.1 s for $f_c = 1$ Hz and $f_c = 10$ Hz, respectively) and hence more droplets impact near the constriction during the closing and opening phase. During the closed phase and start of the opening phase, it is seen that P_c increases so that effects pointed out for $V_L = 0$ ml are emphasized which suggests that a change in mixing fluid properties occurs compared to the closing phase induced by the accumulation of liquid or increased contribution of liquid to the mixture upstream from the constriction. A pulsed jet and subsequent decelerating and starting vortex are formed while the gap starts to widen at the beginning at the opening phase accompanying increased water-air mixing and subsequent upstream liquid evacuation so that eventually mixing properties become similar to the ones characterizing the closing phase. Note that increased mixing following jet deceleration during the opening phase is in agreement with findings for a pulsating jet[19,29] although more research is needed to investigate the contribution of each of the underlying mechanisms. For $f_c = 1$ Hz on the other hand, the effect of jet mixing is less so that properties are re-established more rapidly within the period. Consequently, the main impact of $V_L > 0$ ml is to increase P_c during the closed and opening phase onset due to a change in mixing fluid properties so that the mirror-asymmetry of P_c between the closing and opening phase is enforced as is observed for all frequencies. In addition, for $V_L > 0$ ml, the impact of droplets causes irregular spiking of P_c. Therefore, observed curves are the result of a complex interaction between different phenomena.

B. Two-phase flow models behavior

Experimental observations provide indications that properties of the mixing fluid and flow regime during an oscillation cycle can be altered first by liquid droplet impact along the constriction and second by liquid accumulation, mixing, and removal upstream of the constricted portion following closure. Obviously, these mechanisms contribute to the changes of liquid and gas concentration in the fluid and might affect the flow type as well. In the following, it is sought if and to which extent quasi-one-dimensional models presented in Sec. II allow to explain observed pressure drop tendencies, i.e., estimate $P_c(t)$ for known $P_u(t)$ and $h_c(t) > 0$ mm for all assessed (f_c, V_L) cases. From the description given in Secs. II and IV A, it is *a priori* expected that homogeneous mixing models for gas dominated flow, whether or not corrected for turbulence due to the spatial distribution of droplets, can be used during most of the open phase, closing phase, and opening phase. Near closure, the homogeneous mixing assumption and assumption of gas dominated flow might be less suited so that a separated flow model is *a priori* motivated.

Model accuracies between N measured (P_c) and modeled ($\hat{P}_c$) values for each (f_c, V_L) case are objectively expressed considering the dimensionless coefficient of determination $R^2 \leq 1$ and mean absolute relative error $\xi \geq 0$, given as

$$R^2 = 1 - \frac{\sum_{i=1}^{N}\left(P_c(i) - \hat{P}_c(i)\right)^2}{\sum_{i=1}^{N} P_c^2(i)}, \tag{21}$$

$$\xi = \frac{1}{N}\sum_{i=1}^{N}\left|\frac{P_c(i) - \hat{P}_c(i)}{P_c(i)}\right|. \tag{22}$$

It follows that model outcomes are most accurate when R^2 reaches a maximum (nearest to 1) or when ξ reaches a minimum (nearest to 0). Both R^2 and ξ are considered since experimentally observed instantaneous P_c-spikes associated with liquid droplets which are not modeled, e.g., observed for $f_c = 1$ Hz and $V_L = 5$ ml [Fig. 11(b)], might deteriorate R^2 whereas ξ is less affected. On the other hand, since ξ is relative to the measured value, experimentally observed P_c values in the vicinity of 0 ($P_c \approx 0$) might deteriorate ξ whereas R^2 is less affected.

Resulting R^2 and ξ for most accurate models are summarised in Table II for the closing as well as the opening phase. Note that the open phase is not assessed since viscous flow effects can be neglected. For each case ($f_c \in \{1, 6, 10\}$ Hz), the accuracy of the single-phase airflow model ($V_L = 0$ ml) is given as a reference. As a general tendency, it is found that R^2 and ξ accuracies for $V_L > 0$ ml are similar to those obtained for $V_L = 0$ ml ($R^2 \geq 0.70$ and $\xi \leq 1.4$) so that the quasi-analytical approach can be applied to water-air flow with the same accuracy, as obtained for single phase airflow. Next, selected models indicated in Table II are discussed in more detail for all (f_c, V_L) cases.

For $f_c = 1$ Hz, model accuracies (Table II) observed during closing and opening are alike which is consistent with the mirror symmetry observed on the pressure distribution for all assessed V_L. Most accurate model outcomes are obtained for gas dominated homogeneous flow (6) with Dukler's parameters $\gamma_{i\in\{L,G\}}$ so that $\mu_h = v_f\mu_G + (1 - v_f)\mu_L$ and for gas dominated slip flow (12) for constant C_{LG} [label SG in Fig. 12(a)] with either $C_{LG} = \max(C_{LG}(Lp(D(z))))$ according to (19) or alternatively $C_{LG} = 12$, i.e., Chisholm's constant for laminar-turbulent (LT) liquid-gas flow. Near closure, the gas dominated slip model slightly outperforms the homogeneous flow model as is most notable during the closing phase. This finding holds for all assessed (f_c, V_L) cases. Note that for $V_L \in \{4, 5\}$ ml, R^2 (Table II) decreases (from 0.89 to 0.10) due to the presence of P_c spikes [Fig. 12(a)] whereas $\xi \approx 1.70$ remains.

As for $f_c = 1$ Hz, gas dominated slip (SG) flow (12) for $C_{LG} \approx 12$ provides accurate P_c estimations during the closing phase for $f_c = \{6, 10\}$ Hz. According to (19), C_{LG} is set either constant $C_{LG} = \max(C_{LG}(Lp(D(z))))$ [label SG ($C_{LG} \approx 12$) in Figs. 12(b) and 12(c)] or varying along z as $C_{LG}(z) = (C_{LG}(Lp(D(z))))$ [label SG ($C_{LG}(z)$) in Figs. 12(b) and 12(c)] due to varying hydraulic diameter $D(z)$. From Table II and modeled data curves (SG) illustrated in Figs. 12(b) and 12(c), it is seen that varying $C_{LG}(z)$ gains accuracy as f_c increases from $f_c = 6$ Hz to $f_c = 10$ Hz.

TABLE II. Summary of the best model Eq. (·) and their accuracies (coefficient of determination $R^2 \leq 1$ and mean absolute relative error $\xi \geq 0$): gas dominated slip (SG) model, slip (S) model, and homogenous (H) model and their parameters.

	f_c = 1 (Hz)					
	Closing			Opening		
V_L (ml)	Model	R^2	ξ	Mod	R^2	ξ
0	Air flow	0.83	1.4	Air flow	0.88	0.53
1	(6) H (Dukler)	0.85	1.6	(6) H (Dukler)	0.89	0.46
	(12) SG[a,b]	0.89	0.91	(12) SG[a,b]	0.89	0.42
2	(6) H (Dukler)	0.82	2.4	(6) H (Dukler)	0.83	1.9
	(12) SG[a,b]	0.91	0.78	(12) SG[a,b]	0.83	1.5
3	(6) H (Dukler)	0.77	1.7	(6) H (Dukler)	0.84	0.60
	(12) SG[a,b]	0.85	1.2	(12) SG[a,b]	0.81	0.78
4	(6) H (Dukler)	0.45	2.4	(6) H (Dukler)	0.72	1.56
	(12) SG[a,b]	0.49	1.7	(12) SG[a,b]	0.72	1.47
5	(6) H (Dukler)	0.06	1.7	(6) H (Dukler)	0.17	2.02
	(12) SG[a,b]	0.10	1.3	(12) SG[a,b]	0.16	2.0
	f_c = 6 (Hz)					
	Closing			Opening		
V_L (ml)	Model	R^2	ξ	Mod	R^2	ξ
0	Air flow	0.84	0.70	Air flow	0.70	0.70
1	(12) SG[a,b]	0.87	0.46	(16) S[a,c]	0.90	0.43
	(12) SG[d]	0.90	0.22	Water flow	0.85	0.73
2	(12) SG[a,b]	0.93	0.34	(16) S[a,c]	0.83	0.60
	(12) SG[d]	0.92	0.47	Water flow	0.77	0.46
3	(12) SG[a,b]	0.85	0.31	(16) S[a,c]	0.90	2.5
	(12) SG[d]	0.81	0.34	Water flow	0.80	0.49
4	(12) SG[a,b]	0.96	0.26	(16) S[a,c]	0.85	0.55
	(12) SG[d]	0.97	0.26	Water flow	0.81	0.68
5	(12) SG[a,b]	0.80	0.84	(16) S[a,c]	0.80	1.2
	(12) SG[d]	0.71	1.1	Water flow	0.86	0.51
	f_c = 10 (Hz)					
	Closing			Opening		
V_L (ml)	Model	R^2	ξ	Mod	R^2	ξ
0	Air flow	0.54	0.40	Air flow	0.73	0.83
1	(12) SG[a,b]	0.84	0.29	(6) H (Cicchitti)	0.62	1.2
	(12) SG[d]	0.92	0.23	(9) H (Aung)	0.23	1.7
				(16) S[a,c]	0.91	0.53
2	(12) SG[a,b]	0.82	0.35	(6) H (Cicchitti)	0.52	1.8
	(12) SG[d]	0.77	0.37	(9) H (Aung)	0.078	2.7
				(16) S[a,c]	0.86	1.0
3	(12) SG[a,b]	0.54	4.5	(6) H (Cicchitti)	0.85	0.31
	(12) SG[d]	0.62	4.5	(9) H (Aung)	0.83	1.1
				(16) S[a,c]	0.49	1.5
4	(12) SG[a,b]	0.91	0.24	(6) H (Cicchitti)	0.73	12
	(12) SG[d]	0.96	0.19	(9) H (Aung)	0.44	17
				(16) S[a,c]	0.88	7.2
5	(12) SG[a,b]	0.51	1.4	(6) H (Cicchitti)	0.81	0.52
	(12) SG[d]	0.62	1.3	(9) H (Aung)	0.76	1.1
				(16) S[a,c]	0.60	0.92

[a] C_{LG} (19), constant along z: $C_{LG} = \max(C_{LG}(Lp(z)))$.
[b] Alternatively (12) with Chisholms's constant value: $C_{LG} \approx 12$ (LT flow).
[c] Alternatively (16) with Chisholms's constant value: $C_{LG} \approx 20$ (TT flow).
[d] $C_{LG}(z)$ (19), varying along z: $C_{LG} = C_{LG}(Lp(z))$.

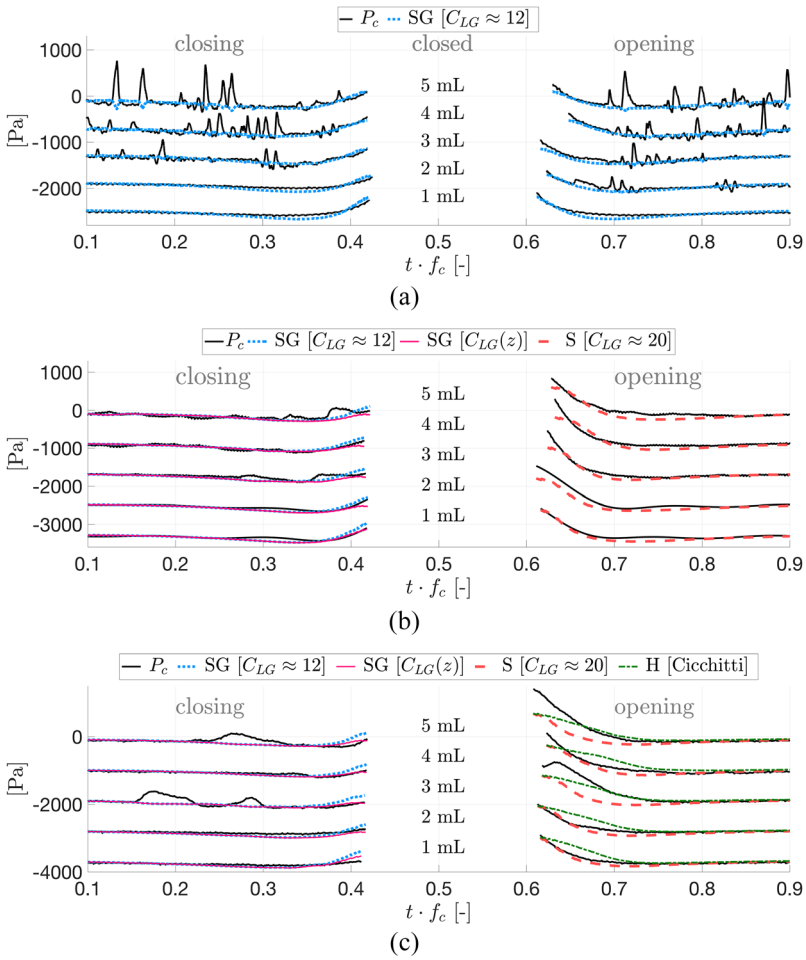

FIG. 12. Measured P_c (black full) and best model outcomes for $V_L \in \{1, 2, 3, 4, 5\}$ ml (shifted for clarity) and $f_c \in \{1, 6, 10\}$ Hz during closing and opening ($h_c > 0$): gas dominated slip (SG) model (12) for $C_{LG} \approx 12$ (thick dotted) or $C_{LG}(z)$ (gray thin full), slip (S) model (16) for $C_{LG} \approx 20$ (thick dashed), and homogenous (H) flow model (6) for Cicchitti parameters (gray thin dashed-dotted) and following Aung (9) (thin dotted). (a) $f_c = 1$ Hz, shifted with 600 Pa; (b) $f_c = 6$ Hz, shifted with 800 Pa; (c) $f_c = 10$ Hz, shifted with 900 Pa.

The gas dominated slip (SG) model is not suitable within the opening phase when $f_c \in \{6, 10\}$ Hz since for all V_L, more accurate P_c estimations are obtained using the slip (S) model (16) with either constant C_{LG} set to max $(C_{LG}(Lp(D(z))))$ according to (19) or alternatively $C_{LG} \approx 20$, i.e., Chisholm's constant for turbulent-turbulent (TT) liquid-gas flow. From Table II, it follows that the slip model is in close agreement with single-phase liquid flow and thus that the flow is no longer gas dominated. For $f_c = 10$ Hz and $V_L \in \{3, 4, 5\}$ ml, the model accuracy is further improved by considering the homogeneous (H) mixing model with parameters $\gamma_{i \in \{L,G\}}$ according to Cicchitti ($\mu_h = x\mu_G + (1 - x)\mu_L$) or homogeneous turbulent flow using (9) (Aung) indicating increased mixture viscosity either generated by increased droplet-induced turbulence or/and jet-related mixing.

Objectively selected liquid-gas models reflect experimental findings and thus the influence of f_c and V_L on water-air mixing and the degree to which mixture viscosity impacts the flow. General tendencies are as follows. During the closing phase and regardless of (f_c, V_L), gas dominated slip (SG) flow (12) provides an accurate flow model when C_{LG} is set in accordance with (19) or alternatively $C_{LG} = 12$ in accordance with laminar-turbulent liquid-gas flow. It is seen that since the hydraulic diameter varies along the channels, the longitudinal z-axis (19) results in overall constant C_{LG} as $C_{LG} = \max(C_{LG}(Lp(z)))$ or C_{LG} is defined locally as $C_{LG}(Lp(z))$. It is seen that this model approach is also suitable during the opening phase for $f_c = 1$ Hz. For imposed oscillation frequencies greater than 1 Hz ($f_c \in \{6, 10\}$ Hz), the mixing is enhanced during the opening phase so that the flow is no longer gas dominated and slip model (16) gains accuracy. Again C_{LG} can be set according to (19) so that it is either constant $C_{LG} = \max(C_{LG}(Lp(z)))$ or locally varying as $C_{LG}(Lp(z))$. When the forced oscillation frequency is further increased to $f_c = 10$ Hz and more liquid is injected $V_L \geq 3$ ml, the homogenous turbulent flow model becomes most accurate since it captures the increased range during which P_c is increased due to enhanced mixing.

V. CONCLUSION

Experimental observations of the pressure within a time-varying constricted portion of a vertical channel show the combined influence of injected water volume $V_L \in \{0, \ldots, 5\}$ ml and imposed oscillation frequency $f_c \in \{1, 6, 10\}$ Hz on water-air mixing and hence on the viscous contribution to the pressure drop. Experimental observations and selected flow models both suggest that the flow remains gas dominated during the closing phase for all assessed (f_c, V_L) whereas during the opening phase, both f_c and V_L affect mixing and hence the mixture viscosity. For $f_c = 1$ Hz, the flow remains gas dominated during the opening phase for all V_L, whereas for $f_c > 1$ Hz, the contribution of water to the mixture increases for all $V_L > 0$ ml so that the flow is no longer gas dominated.

Moreover, for f_c = 10 Hz and $V_L \geq 3$ ml, mixing increases so that the flow becomes homogeneous and turbulent. Further research is necessary to investigate and quantify droplet properties and their distribution and the reciprocal effect on jet and vortex formation and dissipation mechanisms affecting the mixing for different (f_c, V_L). In this study, geometrical and flow parameters were inspired on flow through the human glottis. With respect to glottal flow, it is seen that the common quasi-one-dimensional steady flow model approach can be extended to water-air flow with the same accuracy when viscous mixing is accounted for and differences are observed between the closing and opening phase. It is of interest to further validate selected flow models for different constriction shapes, for self-oscillating deformable glottal replica's as well as to study liquids other than water, i.e., either Newtonian-like contained in some artificial saliva sprays or non-Newtonian-like natural saliva. Furthermore, as suggested by a reviewer, it is of interest to further investigate the role of squeezing flow due to the constricted wall motion on pressure driven channel flow.

ACKNOWLEDGMENTS

This work was partly supported by ArtSpeech Project (No. ANR-15-CE23-0024). X. Pelorson thanks A. Hirschberg for advices on the experimental setup.

[1] Alves, M., Krüger, E., Pillay, B., van Lierde, K., and van der Linde, J., "The effect of hydration on voice quality in adults: A systematic review," J. Voice (published online).
[2] Aung, N. and Yuwono, T., "Evaluation of mixture viscosity models in the prediction of two-phase flow pressure drops," ASEAN J. Sci. Technol. Dev. **29**, 115–128 (2012).
[3] Awad, M. and Muzychka, Y., "Effective property models for homogeneous two-phase flows," Exp. Therm. Fluid Sci. **33**, 106–113 (2008).
[4] Beattie, D. and Whalley, P., "Simple two-phase frictional pressure drop calculation method," Int. J. Multiphase Flow **8**, 83–87 (1982).
[5] Chisholm, D., "A theoretical basis for the Lockhart-Martinelli correlation for two-phase flow," Int. J. Heat Mass Transfer **10**, 1767–1778 (1967).
[6] Chung, P. M. Y., Kawaji, M., Kawahara, A., and Shibata, Y., "Two-phase flow through square and circular microchannels effect of channel geometry," J. Fluids Eng. **126**, 546–552 (2004).
[7] Cicchitti, A., Lombaradi, C., Silversti, M., Soldaini, G., and Zavattarlli, R., "Two-phase cooling experiments—Pressure drop heat transfer burnout measurements," Energ. Nucl. **7**, 407–425 (1960).
[8] Cisonni, J., "Modélisation et inversion d'un système complexe de production de signaux acoustiques," Ph.D. thesis, Grenoble-INP, Grenoble, France, 2008.
[9] Cisonni, J., Van Hirtum, A., Luo, X., and Pelorson, X., "Experimental validation of quasi-one-dimensional and two-dimensional steady glottal flow models," Med. Biol. Eng. Comput. **48**, 903–910 (2010).
[10] Cisonni, J., Van Hirtum, A., Pelorson, X., and Willems, J., "Theoretical simulation and experimental validation of inverse quasi one-dimensional steady and unsteady glottal flow models," J. Acoust. Soc. Am. **124**, 535–545 (2008).
[11] Collier, J. and Thome, J., *Convective Boiling and Condensation* (Claredon Press, 1994), p. 640.
[12] Davidson, W., Hardie, P., Humphreys, C., Markson, A., Mumford, A., and Ravese, T., "Studies of heat transmission through boiler tubing and pressures from 500-3300 lbs," J. Fluids Eng. **65**, 553–591 (1943).
[13] Deverge, M., Pelorson, X., Vilain, C., Lagré, P., Chentouf, F., Willems, J., and Hirschberg, A., "Influence of collision on the flow through *in-vitro* rigid models of the vocal folds," J. Acoust. Soc. Am. **114**, 3354 (2003).
[14] Dukler, A., Moye, W., and Cleveland, R., "Frictional pressure drop in two-phase flow," AIChE J. **10**, 38–51 (1964).
[15] Fourar, M. and Bories, S., "Experimental study of air-water two-phase flow through a fracture (narrow channel)," Int. J. Multiphase Flow **21**, 621–637 (1995).
[16] Fries, D., Trachsel, F., and von Rohr, P., "Segmented gas-liquid flow characterization in rectangular microchannels," Int. J. Multiphase Flow **34**, 1108–1118 (2008).
[17] Fujiki, R., Chapleau, A., Sundarrajan, A., McKenna, V., and Sivasankar, M., "The interaction of surface hydration and vocal loading on voice measures," J. Voice **31**, 211–217 (2017).
[18] Garcia, F., Garcia, R., Padrino, J., Mata, C., Trallero, J., and Joseph, D., "Power law and composite power law friction factor correlations for laminar and turbulent gas-liquid flow in horizontal pipelines," Int. J. Multiphase Flow **29**, 1605–1624 (2003).
[19] Grosshans, H., Szasz, R., and Fuchs, L., "Enhanced liquid-gas mixing due to pulsating injection," Comput. Fluids **107**, 196–204 (2015).
[20] Hanratty, T., *Physics of Gas-Liquid Flows* (Cambridge University Press, 2013), p. 333.
[21] Kandlikar, S., "Fundamental issues related to flow boiling in minichannels and microchannels," Exp. Therm. Fluid Sci. **26**, 389–407 (2002).
[22] Kashinsky, O., "Experimental study of laminar bubbly flows in a vertical pipe," Exp. Fluids **15**, 308–314 (1992).
[23] Lee, H. and Lee, S., "Pressure drop correlations for two-phase flow within horizontal rectangular channels with small heights," Int. J. Multiphase Flow **27**, 783–796 (2001).
[24] Li, X. and Hibiki, T., "Frictional pressure drop correlation for two-phase flows in mini and micro single-channels," Int. J. Multiphase Flow **90**, 29–45 (2017).
[25] Lin, S., Kwok, C., Li, R., Chen, Z., and Chen, Z., "Local frictional pressure drop during vaporization for R-12 through capillary tubes," Int. J. Multiphase Flow **17**, 95–102 (1991).
[26] Lockhart, P. and Martinelli, R., "Proposed correlation of data for isothermal two-phase two-component flow in pipes," Chem. Eng. Prog. **45**, 39–48 (1949).
[27] McAdams, W., Woods, W., and Heroman, L., "Vaporization inside horizontal tubes II-benzene-oil mixtures," J. Fluids Eng. **64**, 193–200 (1942).
[28] Mishima, K. and Hibiki, T., "Some characteristics of air-water two-phase flow in small diameter vertical tubes," Int. J. Multiphase Flow **22**, 703–712 (1996).
[29] Muculus, M., "Entrainment waves in decelerating transient turbulent jets," J. Fluid Mech. **638**, 117–140 (2009).
[30] Muzychka, Y. and Awad, M., "Asymptotic generalizations of the Lockhart-Martinelli method for two phase flows," J. Fluids Eng. **132**, 031302 (2010).
[31] Owen, W., "Two-phase pressure gradient," in *ASME International Developments in Heat Transfer, Part II* (ASME, 1961), pp. 363–368.
[32] Sato, Y. and Sekoguchi, K., "Liquid velocity distribution in two-phase bubbly flow," Int. J. Multiphase Flow **2**, 79–95 (1975).
[33] Trela, M., Kwidzinski, R., and Lackowski, M., "Generalization of Martinelli-Nelson method of pressure drop calculation in two-phase flows," E3S Web Conf. **13**, 02006 (2017).
[34] Van Hirtum, A., "Analytical modeling of constricted channel flow," Mech. Res. Commun. **83**, 53–57 (2017).
[35] Van Hirtum, A., Cisonni, J., and Pelorson, X., "On quasi-steady laminar flow separation in the upper airways," Commun. Numer. Methods Eng. **25**, 447–461 (2009).
[36] Verdolini-Marston, K., Titze, I., and Druker, D., "Changes in phonation threshold pressure with induced conditions of hydration," J. Voice **4**, 142–151 (1990).
[37] Vilain, C., Pelorson, X., Fraysse, C., Deverge, M., Hirschberg, A., and Willems, J., "Experimental validation of a quasi-steady theory for the flow through the glottis," J. Sound Vib. **276**, 475–490 (2004).
[38] Wallis, G., *One Dimensional Two Phase Flow* (McGraw-Hill, New York, 1969), p. 408.
[39] Wu, B., Van Hirtum, A., and Luo, X., "Pressure driven steady flow in constricted channels of different cross section shapes," Int. J. Appl. Mech. **5**, 1350002 (2013).
[40] Xu, Y., Fang, X., Su, X., Zhou, Z., and Chen, W., "Evaluation of frictional pressure drop correlations for two-phase flow in pipes," Nucl. Eng. Des. **253**, 86–97 (2012).
[41] Zhang, W., Hibiki, T., and Mishima, K., "Correlations of two-phase frictional pressure drop and void fraction in mini-channel," Int. J. Heat Mass Transfer **53**, 453–465 (2010).
[42] Zhao, T. and Bi, Q., "Pressure drop characteristics of gas-liquid two-phase flow in vertical miniature triangular channels," Int. J. Heat Mass Transfer **44**, 2523–2534 (2001).